THE ASTRONOMICAL JOURNAL VOLUME 112, NUMBER 1 JULY 1996

SPECTRAL IRRADIANCE CALIBRATION IN THE INFRARED. VI. 3–35 μm SPECTRA OF THREE SOUTHERN STANDARD STARS

MARTIN COHEN

Jamieson Science and Engineering, Inc., Suite 204, 5321 Scotts Valley Drive, Scotts Valley, California 95066, and Radio Astronomy Laboratory, 601 Campbell Hall, University of California, Berkeley, California 94720
Electronic mail: cohen@bkyast.berkeley.edu

FRED C. WITTEBORN, JESSE D. BREGMAN, AND DIANE H. WOODEN

Space Science Division, Mailstop 245-6, NASA-Ames Research Center, Moffett Field, California 94035
Electronic mail: (witteborn, bregman, wooden)@ssa1.arc.nasa.gov

ALBERTO SALAMA AND LEO METCALFE

ISO Science Operations Centre, Astrophysics Division of ESA, Villafranca, Spain
Electronic mail: (asalama, lmetcalf)@iso.vilspa.esa.es

Received 1995 December 27; revised 1996 March 27

ABSTRACT

We present three new absolutely calibrated continuous stellar spectra from 3 to 35 μm, constructed as far as possible from actual observed spectral fragments taken from the *Kuiper Airborne Observatory (KAO)*, and the *IRAS* Low Resolution Spectrometer (LRS). These stars—α^1 Cen, α TrA, and ϵ Car—augment our previous archive of complete absolutely calibrated spectra for northern K and M giants. All these spectra have a common calibration pedigree. The wavelength coverage is ideal for calibration of many existing and proposed ground-based, airborne, and satellite sensors. *KAO* and *IRAS* data in the 15–30 μm range suggest that the spectra of cool giants are close to Rayleigh–Jeans slopes. Our observations of α^1 Cen, absolutely calibrated via our adopted Sirius model, indicate an angular diameter in very good agreement with values in the literature, demonstrating "closure" of the set of spectra within our absolute framework. We compare our observed α^1 Cen spectrum with a published grid of theoretical models from Kurucz, and adopt a plausible theoretical shape, that fits our spectrum, as a secondary reference spectrum in the southern sky.

1. INTRODUCTION

In this ongoing series of papers we have described a consistent effort to provide absolutely calibrated broad and narrowband infrared photometry based upon a carefully selected, infrared-customized pair of stellar models for Vega and Sirius, created by Kurucz, and absolutely calibrated by Cohen *et al.* (1992, hereafter referred to as Paper I). These hot stellar models have been employed as reference spectra to calibrate six K and M giants using the methods detailed by Cohen *et al.* (1992, hereafter referred to as Paper II) and Cohen *et al.* (1995, hereafter referred to as Paper IV).

In the present paper we extend these techniques to the southern hemisphere to meet several different objectives. Our primary standard, Sirius, is best observed from the south, and we wished to intercompare this star and the infrared-brighter solar-type star, α^1 Cen (HR 5459=HD 128620; G2 V), for which Kurucz (1995) has kindly provided us with his grid of atmospheric models (published by Furenlid & Meylan 1990). The salient issue is that we wished to find, empirically, a model that fits our low-resolution infrared spectral observations and to use it as an interpolator to smoothe our spectrum of α^1 Cen, and as an extrapolator to somewhat longer wavelengths. Our finally adopted model (Sec. 4) not only provides an adequate match to the CO fundamental region, its overall shape also satisfies the independent photometry between 1.2 and 12.5 μm. To this extent, we have achieved our goal of offering a brighter calibrator in the south than Sirius, for use at low resolution and on small telescopes such as those on satellites. The purpose of this paper is not to determine atmospheric abundances in α^1 Cen, nor to offer the definitive model for this star, but merely to use our observations to select a plausible theoretical shape for its spectral energy distribution.

We wanted to increase the spectral resolution of our calibration standards beyond the lower-resolution products recently released as Paper IV, and to enlarge the set of K-giant spectral types so far studied. The cool stars α TrA (HR 6217=HD 150798: K2 III), and ϵ Car (HR 3307=HD 71129: K3 III) were judged ideal candidates for the *KAO* flights focusing on Sirius, so that they could be compared directly with our primary standard.

A particular goal of these flights was the acquisition of 15–30 μm spectra from the *KAO* through the use of Si:P BIB detectors provided by ESTEC. However, we found that Sirius, our primary reference, provided insufficient signal-to-noise ratios for work at these long wavelengths. We, therefore, made an effort to use the brighter α^1 Cen as a secondary

 0004-6256/96/112(1)/241/11/$6.00

reference star for these difficult observations. We hoped to test the general conclusion reached in Papers II and IV that cool giants appear essentially flat in $\lambda^4 F_\lambda$ space, justifying our use of the Engelke (1992) approximation to smoothe and/or extrapolate our observed spectra as far as 35 μm (see Sec. 5).

2. THE NEW SPECTRAL FRAGMENTS

All the new spectral fragments incorporated in this paper were secured with the NASA-Ames "HIFOGS" (High-efficiency Infrared Faint Object Grating Spectrometer: Witterborn *et al.* 1995) on the *KAO*. We augmented our usual 1×120 set of Si:Bi linear arrays by two Batelle 1×32 Si:P detectors, combining the Si:P arrays into 32 separate readouts of two detectors each. These observations were secured during three flights of the *KAO* while based in Christchurch, New Zealand. The flight dates were 1993 April 7, 9, and 12 UT. Confirming data on the ratios of α^1 Cen and α TrA to α CMa were acquired in 1994 July with HIFOGS from Australia, during *KAO* flights to observe the encounter of Comet Shoemaker–Levy with Jupiter. While these later flights do support the spectral shapes and flux density levels for these two program stars obtained from New Zealand, the observing time per star was significantly less in Australia. These 1994 data thus confirm our 1993 work but without contributing much statistical significance to a combination with the 1993 spectra.

Our methodology for creating a complete and continuous composite spectrum from 1.2 to 35 μm is described in detail in Papers II and IV. However, the paucity of infrared photometric and spectral measurements of these southern objects dictated a modified approach to the assembly of complete spectra. It is unfortunately the case that the vital northern archive constructed from the Lear jet and *KAO* by Strecker *et al.* (1979) using CVF spectrometers has no counterpart in the south, nor has the work been extended to any other stars even in the north. Consequently, we secured a grating and appropriate order-sorting filter to provide our own contemporaneous 2.9–5.5 μm spectral fragments.

No preexisting, ground-based 10 μm spectral observations could be located so we employed a grating to provide *KAO* 9–13 μm spectroscopy. We realized that on the *KAO* these were likely to have quite poor signal-to-noise but felt that they offered an independent appraisal of the LRS spectra and might assist in splicing 5–9 μm fragments to the LRS spectra. LRS data already existed for all three stars. To extend the wavelength coverage toward 30 μm, and supplement noisy LRS data, we used four overlapping grating settings for the 15–30 μm region. These provided coverage from 15.0 to 18.5 μm on the Si:Bi array (two settings), and 19.5–27.2 μm on the Si:P arrays (two settings).

The method used to build the new composites varied according to the existence or absence of characterized mid-infrared photometry. Given narrowband photometry in the 10 μm region, we proceeded exactly as in Papers II and IV. In the absence of such photometry we resorted to an "end-to-end" method by splicing the 5–9 μm piece onto the photometrically constrained 2.9–5.5 μm fragment, then further splicing the 9–13 μm and LRS pieces onto these. This latter scheme clearly provides less control over the radiometric aspect of a composite. Everything now turns on the near-infrared photometry (which might be in a single passband) and the fidelity of the shapes of the succeeding fragments in their regions of overlap. But this was judged to be the sole approach available to us in the absence of 10 μm photometry.

TABLE 1. Engelke functions used in our composite spectra.

Star	Effective temperature (K)	Angular diameter (mas)
α^1 Cen	5770	8.58
α TrA	4140	9.55
ϵ Car	4064	12.67

As in Paper IV, we chose to substitute the best-fitting Engelke function for noisy 10–20 μm data. The essential parameters for the Engelke approximations, namely, effective temperature and angular diameter, were initially fixed by reference to the literature. Specifically, we took the following parameters: for α^1 Cen, 5770 K and a radius from Lydon *et al.* (1993), and a distance from Demarque *et al.* (1986), implying an angular diameter of 8.66 milliarcsec (mas); for α TrA, 4140 K and 12.4 mas (Harper 1992); for ϵ Car, 4064 K (Pasquini & Brocato 1992), and we guessed 12.5 mas. As in previous work, $T_{\rm eff}$ is never altered; and the angular diameter is redetermined when the Engelke function is spliced to our observed spectra. We do, however, assign an additional uncertainty to any usage of this approximation, driven by the uncertainties in both $T_{\rm eff}$ and angular diameter (cf. Blackwell *et al.* 1991), but also taking note of the change in infrared slope of the Engelke function engendered by a typical uncertainty of $\pm$100 K in stellar effective temperature.

Table 1 summarizes our adopted values of $T_{\rm eff}$ and our determination of angular diameters via Engelke approximations fitted to our observed spectra. For α^1 Cen, our estimate is very close to expectation yet that for α TrA is highly discrepant with Harper's (1992) value. However, Harper is vague on the method used to determine α TrA's diameter. This star entirely lacks any published near-infrared photometry so his reference to use of the "infrared flux method" (hereafter referred to as IRFM) is odd, to say the least. From the language of the relevant paragraph of Harper (1992) we deduce that he used V with Johnson colors to estimate near-infrared photometry, for a spectral type of K4 III. The literature on this star prefers a type of K2 and we estimate that the application of Johnson K4 colors rather than those for type K2 could have led to overestimates of the "observed" near-infrared flux densities by about 60%, thereby raising the monochromatic derivations of angular diameter (following Blackwell *et al.* 1991) by about 26%. Correcting Harper's diameter for this overestimate yields about 9.8 mas, close to our value. Whether this is the correct reconstruction of Harper's line of reasoning or not, it is clear that any method that applies the IRFM to a star without observed infrared magnitudes must be regarded as highly unreliable. There is also support for a much lower value than Harper's in the work of Kovacs (1983), where a value of 15 mas is cited for this star

solely based on Wesselink *et al.*'s (1972) $(V,B-V)$ approach. The equivalent parallax deduced by these authors is 0.043 arcsec, yet the average of the three values now available in the literature [0.024, 0.027 (from SIMBAD), and 0.031 arcsec from the *Yale Bright Star Catalog* (Hoffleit 1982)] is 0.027 arcsec. Following Kovacs' (1983) approach, such a parallax would then be equivalent to a diameter of 9.4 mas, very close to our deduced value.

3. SUPPORTING PHOTOMETRY AND THE NEW COMPOSITES

The absence of high-quality near-infrared photometry through characterized passbands was addressed through *JHKL* measurements made for this study by Carter (1994) at the *South African Astronomical Observatory* (hereafter referred to as *SAAO*). For α^1 Cen, we also used the *ESO L* and *M* magnitudes of Engels *et al.* (1981), and two measurements made in the 10 μm region with the *ESO* narrowband filters "*N*1" and "*N*2" (Bouchet *et al.* 1989). We have multiplied these published passbands (*ESO User's Manual*) by our calculated representative atmosphere for the La Silla site. Zero points were traced for all the *ESO* passbands through published observations of Sirius by these same authors. All photometry used to construct the three composites appears in the individual informational headers in Tables 2–4, after correction for zero points. These data provided the scale factors that best match spectral fragments to the observed in-band fluxes from photometry, and the local "biases" of those fragments, i.e., the uncertainties associated with each scale factor. Biases, therefore, are correlated errors that refer to entire ranges of the overall spectrum, rather than the uncorrelated errors that are specific to each individual wavelength point. Two kinds of bias occur: "local" biases arising from scaling of spectral fragments; and "global" that derive directly from the underpinning uncertainty in the absolute calibrations of Vega and Sirius (Paper I).

The standard technique of Papers II and IV was applied to the composite of α^1 Cen. For α TrA and ϵ Car, where we have no ground-based photometry beyond 4 μm, we pinned our 3–5.5 μm *KAO* fragment to Carter's *L* point and employed the end-to-end approach described above. Tables 2–4 reproduce the calibration pedigrees that accompany the three new composite spectra, including all pertinent information on the processes undertaken during assembly of these composites, with their results (scale factors and biases). The date of original assembly appears, along with details of the photometry used to calibrate the composite radiometrically. The FWHM of the relevant passbands and their effective wavelengths for our Vega spectrum and for the star in question are recorded, along with the monochromatic specific intensities. All archival spectral fragments are detailed, with their total spectral ranges, the ranges of their data that were actually utilized, and their average resolving power over that spectral range (expressed as the ratio of $\lambda/\Delta\lambda$).

All the *KAO* spectral fragments were processed so as to remove residual terrestrial atmospheric features by computing atmospheric transmission spectra [through use of Lord's (1992) "ATRAN" tool] pertinent to the actual airmass and column of precipitable water vapor in the line of sight at the time of each stellar observation. In the wavelength region of principal interest, where our spectra were used to construct the composites, these corrections for residual telluric absorptions did not exceed about 3% (we exclude the CO_2 region near 4.3 μm, opaque even at *KAO* altitudes). At the longest wavelengths where water vapor dominates, the maximum typical correction was about 5% (near 28 μm), excluding the CO_2 near 15 μm, also opaque from the *KAO*.

We prefer to provide pristine data whenever possible, rather than to regrid each composite to some equally spaced or common wavelength scale. In the AAS CD-ROM series that will carry the tables from the present paper, each stellar composite spectrum, therefore, has a different set of wavelengths. We tabulate: wavelength (in μm); monochromatic specific intensity (F_λ in units of W cm^{-2} μm^{-1}); total uncertainty (also in units of W cm^{-2} μm^{-1}) associated with this value of F_λ; local bias (in %); and global bias (in %). For most applications, "total uncertainty" is the error term most appropriate to use. It is the standard deviation of the spectral irradiance and includes the local and global biases. Local and global biases are given as a percentage of the irradiance. The global bias does not contribute error to flux ratios or color measurements, and may be removed (in the root-sum-square sense) from the total error.

Some remarks are in order with respect to α Cen, because of its composite character. The star consists dominantly of a G2 V, with a K1 V companion separated by about 18″, and differing in *V* mag by 1.34^m. On the *KAO* we used a 20″ diameter aperture which avoided the K dwarf star. For identical reasons, the *SAAO* photometry was taken with a 17″ aperture (half the usual diameter for Carter's work). But the *IRAS* flux densities at 12 and 25 μm will clearly refer to both G and K dwarf components, as will the LRS spectrum. It is, therefore, important to assess the degree of contamination of the LRS spectrum by the K star and to determine whether the K star and G star may have differently shaped energy distributions. For this purpose we have reviewed the photometry for the two separate components of α Cen secured by Thomas *et al.* (1973) at wavelengths from *J* to 11.2 μm. Below *J*, one expects strong temperature-related differences in the stellar energy distributions but, between 1.6 and 11.2 μm, the average difference in brightness between the G and K stars is 0.91^m, and it appears independent of wavelength, within the estimated uncertainties. In particular, the same difference in magnitude is observed at 8.4 as at 11.2 μm. Therefore, we deduce: (i) that the G2 V and K1 V components contribute 70% and 30% of the light, respectively, at all wavelengths between 1.6 and 11.2 μm, and (ii) that neither star has the SiO band in absorption, or there is no difference in SiO fundamentals between the two stars. Consequently, the LRS spectrum has the correct shape for the G2 V component even though the flux density level is wrong (based on simulations with Kurucz model atmospheres for the two dwarf components). Therefore, we were able to construct the 3–35 μm spectrum of α^1 Cen by our normal techniques, using spectra calibrated through ratios to Sirius in the several spectral regions, extended by an appropriate Engelke approximation [Fig. 1(a)], but not using the new long wave (>15 μm) *KAO* measurements (Sec. 5).

TABLE 2. "Header" information accompanying α^1 Cen composite.

5-9-95 OBSERVED SPECTRUM OF ALPHA[1] CENTAURI

α^1 Cen photometry file: photometry actually used to construct the spectrum

Name	FWHM (μm)	Mag.±Unc.	Eff Wvl (Vega) (μm)	Eff Wvl (star) (μm)	F_λ (W cm^{-2} μm^{-1})	Source
SAAO-L	0.5648	−1.559±0.015	3.475	3.450	3.00E-14	Carter 1994
ESO-L	0.6509	−1.552±0.021	3.768	3.768	2.18E-14	Engels *et al.* 1981
ESO-M	0.5418	−1.437±0.028	4.748	4.759	7.95E-15	Engels *et al.* 1981
ESO-N1	0.8954	−1.557±0.023	8.394	8.394	9.68E-16	Bouchet *et al.* 1989
ESO-N2	1.2949	−1.553±0.026	9.886	9.853	5.06E-16	Bouchet *et al.* 1989

Spectral fragments and portions of these actually used in observed spectrum ("used" may include combination with other data where overlaps occur)

Fragment	Reference	Total range (μm)	Start and stop wavelengths (μm)	Average resolving power
KAO-NIR	1	3.04–5.53	3.04–5.53	160
KAO-5–9	2	5.07–9.28	5.07–9.28	190
KAO-8–13	3	8.80–13.07	···	250
LRS	4	7.67–22.74	7.67–11.55	30
KAO-Si:Bi	5	15.00–18.51	···	80
KAO-Si:P	6	19.48–27.20	···	180
LONG	7	1.25–35.00	12.20–35.00	

References:

(1),(5),(6) HIFOGS data of 1993 April 10 & 12 *KAO* flights [α^1 Cen/α CMa].

(2),(3) HIFOGS data of 1993 April 7 *KAO* flight [α^1 Cen/α CMa]. Spectral ratios in both these wavelength ranges are additionally confirmed by HIFOGS data of 1994 July 22 *KAO* flight from Australia.

(4) LRS raw data extracted from "LRSVAX" Groningen archive at NASA-Ames.

(7) Engelke Fn. used for T=5770 K and ang. diam. of 8.66 mas [see Lydon *et al.* (1993) and Demarque *et al.* (1986)]; we rescaled this to 8.59 mas. This Engelke function was locked to the photometrically scaled LRS spectrum by splicing and used to replace the observations from 12.20 μm. An error of 2.0% in EFn. due to effective temperature uncertainty was input for this fragment.

INFORMATION ON SPLICES AND BIASES INCURRED

Process	Factor determined	±Bias (%)
NIR cf. photometry	0.796	1.31
LRS blue/red bias	···	0.09
LRS cf. photometry	0.778	2.07
5–9 joint splice to	···	
NIR and LRS	0.995	0.16
Engelke Fn. splice to LRS	0.989	0.38

We proceeded to assemble composites for α TrA and ϵ Car based on calibration of their spectra ratioed to that of Sirius. However, once we had selected a model atmosphere for α^1 Cen (see Sec. 4), we were able to recalibrate the observed spectral fragments for these two K giants using ratios to α^1 Cen instead, which yielded higher signal-to-noise data. The overall shapes of the composites based entirely on Sirius agree well with the less noisy ones built through α^1 Cen. In this paper we present solely the latter spectral composites for α TrA and ϵ Car. Figure 1 presents all three stellar composites in the form of absolute $\log(\lambda^4 F_\lambda)$ plots against $\log(\lambda)$. In each spectrum, the $\pm 1\sigma$ error range is indicated, as is the relevant scaled Engelke approximation used for smoothing and extrapolation purposes. Overplotted in each figure are the photometric points used to assemble the relevant spectrum (filled squares), together with the *IRAS* Faint Source Survey (Moshir *et al.* 1992) points (unused in the process of spectral assembly: filled triangles), and the long-wavelength points we derived from our *KAO* spectra (see Sec. 5: open squares). Each photometry point is plotted at its isophotal wavelength for the particular star, with horizontal bars that represent the extent of its FWHM (not necessarily symmetric with respect to the isophotal wavelength), and vertical bars that indicate the uncertainty in the photometry.

Figure 1(a) shows an apparent discrepancy between the M-band point of Engels *et al.* (1981) and our *KAO* spectroscopy of α^1 Cen. However, Table 2 indicates that the 1σ uncertainty of this 4.7 μm point is the largest of the errors for the five photometric points that we used to build the composite spectrum. The difference between the integrated in-band flux when this passband is run over our spectrum and the ground-based 4.7 μm in-band flux is significant only at the 2σ level. Further, photometry in the 5 μm window is notoriously difficult from relatively low-altitude sites on the ground such as La Silla. It has also been somewhat problem-

TABLE 3. "Header" information accompanying α TrA composite.

12-5-95 OBSERVED SPECTRUM OF ALPHA TRIANGULI AUSTRALIS
α TrA photometry file: photometry actually used to construct the spectrum

Name	FWHM (μm)	Mag.±Unc.	Eff Wvl (Vega) (μm)	Eff Wvl (star) (μm)	F_λ (W cm^{-2} μm^{-1})	Source
SAAO-L	0.5648	−1.338±0.008	3.475	3.463	2.45E-14	Carter 1994

Spectral fragments and portions of these actually used in observed spectrum ("used" may include combination with other data where overlaps occur)

Fragment	Reference	Total range (μm)	Start and stop wavelengths (μm)	Average resolving power
KAO-NIR	1	2.90–5.51	2.90–5.51	160
KAO-5–9	2	4.94–9.36	4.94–9.36	190
KAO-8–13	3	8.80–13.08	...	250
LRS	4	7.67–22.74	7.67–12.59	30
KAO-Si:Bi	5	15.00–18.51	...	80
KAO-Si:P	6	21.90–27.08	...	180
LONG	7	1.25–35.00	11.00–35.00	

References:
(1),(5),(6) HIFOGS data of 1993 April 10 & 12 *KAO* flights [α TrA/α^1 Cen] and [α TrA/α CMa].
(2),(3) HIFOGS data of 1993 April 7 *KAO* flight [α TrA/α^1 Cen] and [α TrA/α CMa]. The 5–9 μm spectral ratio is additionally confirmed by HIFOGS data of 1994 July 22 *KAO* flight from Australia.
(4) LRS raw data extracted from "LRSVAX" Groningen archive at NASA-Ames.
(7) Engelke Fn. used for T=4140 K and ang. diam. of 12.40 mas (Harper 1992); we rescaled this to 9.55 mas. This Engelke function was locked to the photometrically scaled LRS spectrum by splicing and used to replace the observations from 11.00 μm. An error of 2.6% in EFn. due to effective temperature uncertainty was input for this fragment.

INFORMATION ON SPLICES AND BIASES INCURRED

Process	Factor determined	±Bias (%)
KAO-NIR cf. photometry	1.004	0.74
KAO-5–9 splice to NIR	1.050	0.14
LRS blue/red bias	...	0.06
LRS splice to *KAO*	1.009	0.40
Engelke Fn. splice to LRS	0.593	0.78

atic to trace the exact cold filter profiles for the *ESO* photometers due to their rapid evolution during the late 1970s and early 1980s (van Dijsseldonk 1994). We, therefore, see no reason for concern at this separation in the figure.

4. THE SPECTRUM OF α^1 CEN AND THE KURUCZ MODEL

Although it had been our original intention to compare all stars directly with Sirius, the signal-to-noise actually obtained on Sirius longward of the 10 μm region was rather poor for this purpose. Consequently, we decided to compare program stars also with α^1 Cen, which is significantly brighter.

We wanted to test the internal consistency of our spectra of Sirius and α^1 Cen, in order to establish the latter as a viable southern reference star. Examination of the generic grid of model atmospheres by Kurucz (1991) indicated that models for 5770 K and log g of 4.30 with varying metallicities differ almost negligibly in the shape of their infrared continua; the only obvious distinction is in the strengths of the CO bands, primarily the fundamental. It was clear from the Kurucz grid that generic models of α^1 Cen with normal solar abundances would fit our data better than those with nonsolar abundances.

To assess the probable value of the Kurucz model for α^1 Cen in the infrared, one should directly test the Kurucz model of the Sun against the highest-resolution solar infrared observations. The great similarity of physical characteristics of the Sun and α^1 Cen suggests the relevance of such a test, particularly if it addresses the 5 μm region, where ground-based spectroscopy is scarce. Farmer & Norton (1989) observed the Sun from the Space Shuttle, using the "ATMOS" Fourier Transform Spectrometer. They have provided us with their archival spectra of the solar intensity integrated through a circular diaphragm centered on the disk and extending out to μ=0.951. We have abstracted portions of their data in the 5 μm region where a plethora of CO lines dominates the solar spectrum. In this wavelength region, the resolving power is 136 000. Kurucz (1996) has very kindly computed his spectrum of the Sun using the SYNTHE spectrum synthesis program and line data from the CD-ROM 18 (Kurucz 1993a). The model is the theoretical solar model from the CD-ROM 13 (Kurucz 1993b). The spectrum was computed for a range of angles on the disk and rotationally

overall effect if Kurucz had switched line lists in these models. [It is, of course, possible that the newer CO line strengths might be systematically different from those of Kirby-Docken & Liu (1978), and an updated CO archive alone could remove the small discrepancies between computed and observed line depths in Fig. 2.]

Microturbulent velocity in all models is 2.0 km s^{-1} and convection is treated using *L/H* of 1.25. Although Furenlid & Meylan determined a *vturb* of 1 km s^{-1}, our increase makes up for missing line opacity in the model due to the under-representation in the line list of the heavy elements. Because all our potential applications for this model are at low resolution, we chose this model's *vturb*. However, we have examined the consequences had we used a grid with 1 km s^{-1}, instead of the 2 km $^{-1}$ version. To quantify the maximum expected effect, we have compared two models with C and O both enhanced by +0.2 over solar, one with 2 km s^{-1}, and its otherwise identical counterpart with 1 km s^{-1}, to see by how much the 1 km s^{-1} model would have reduced the CO fundamental's depth computed for *vturb* of 2 km s^{-1}. In the IR region where we have data, we find essentially no difference between the two full-resolution calculations that exceeds 0.9%, and degradation of the two models to match our observed resolution lessens this maximal difference to only 0.6%. For the model we finally selected, with much less C and O than this trial calculation (solar, or 0.1 dex below solar), this difference would be appreciably diminished. The maximum expected difference, of course, always occurs close to 4.6 μm and, for our adopted model, is much smaller than both the difference between models with [0.0] and [−0.1], and our observational 1σ uncertainties. Consequently, we would not have selected a model with significantly different attributes were we to have used the grid with 1 km s^{-1}.

Figure 3 compares the emergent spectra for four of the models in our grid (with C and O abundances of −0.2, −0.1, 0.0, and +0.1 with respect to solar) with the *KAO* spectrum of α^1 Cen near the CO fundamental (to facilitate direct comparison we smoothed the *KAO* data and each model by a Gaussian with FWHM of 0.2 μm, and regridded the models to exactly the same wavelength scale as the observed spectra. To the eye, the two models closest in shape to the observations are those with solar C and O, and with C and O both set 0.1 dex below solar. The other two models bracket the observed spectral shape and serve to quantify the variation in the CO fundamental band with these different abundances.

We have compared the shapes of the emergent spectra for these four models with our *KAO* spectrum for α^1 Cen by performing a differential quantitative analysis of the match of shape between each model and the observed spectrum to determine the best-fitting model. In this analysis, each model is allowed to vary up and down freely of the others in order to provide the best fit for that model. Figure 3 simply presents the spectra in such a way as to enhance their differences in the CO fundamental and show their great similarity outside this region. Figure 3 does *not* indicate the actual best-fit scale factors obtained. The nature of these tests was to find both the best multiplier (equivalent to the stellar angular subtense: corresponding to the χ^2 minimum over the

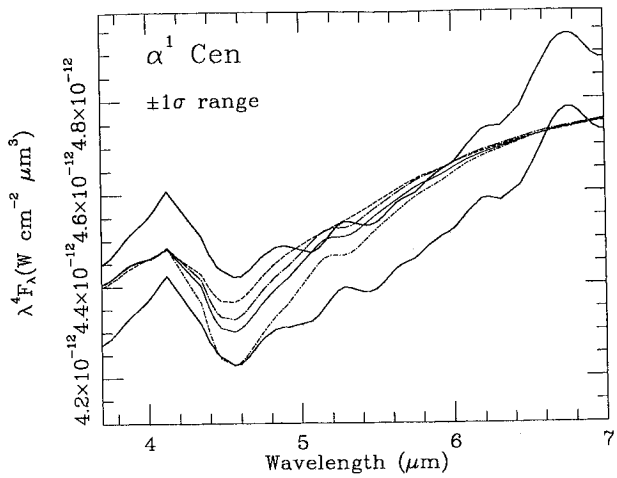

FIG. 3. The ±1σ range around our observed composite spectrum of α^1 Cen in the region of the CO fundamental, plotted in $\lambda^4 F_\lambda$ space, and compared with four models from our Kurucz grid for this star. Each model is scaled to the same solid angle (corresponding to 8.58 mas) and smoothed by a Gaussian of 0.2 μm FWHM, as is the observed spectrum in this figure. The models, from top to bottom, are for C and O abundances of −0.2, −0.1, 0.0, and +0.1 dex, with respect to solar.

set of possible scale factors) and, more importantly, the "bias" (the uncertainty in scaling factor for the best fit: cf. Paper IV). A large uncertainty implies a poor match in shape because the range of acceptable multipliers is wide, whereas a small uncertainty implies a good match in shape. This uncertainty is determined directly from the formal χ^2 parabola and is related to the breadth of the parabola and, as such, is an independent assessment.

These tests were applied to several wavelength ranges. When tested over a broad wavelength range (e.g., 3–12 μm), essentially all models fit equally well. However, emphasizing the region with the greatest observed spectral structure (Fig. 3) provides quantitative discrimination. In particular, varying the wavelength region of comparison from a minimum range of 4.1–5.2 μm to a maximum of 3.3–7.1 μm produced curves of minimum χ^2 value and uncertainty in multiplier with well-defined minima lying between the [0.0] and [−0.1] models, while the [+0.1] and [−0.2] models always fit significantly more poorly. We see no statistically significant distinction between the [0.0] and [−0.1] and are, therefore, unable to discriminate more precisely between the two closest matching models, given the uncertainties in our observed spectral shape. Therefore, we simply averaged the two emergent spectral energy distributions, which differ by at most 1% across our entire observed range, 3–30 μm (the greatest divergence is, of course, confined to the region near 4.6 μm). We took this averaged emergent spectral shape as the best model representation for this star. Figure 4 represents the ratio of our observations to the absolutely calibrated version of this model (see below), near the CO fundamental; observations and model were smoothed by a Gaussian with 0.2 μm FWHM to produce Fig. 4. This presumably corresponds to values of C and O enhancement between 0.0 and −0.1, if these were to vary in unison, as we have assumed. We emphasize that we have not determined the C and O abundances for this star; rather, we have chosen a physically defensible

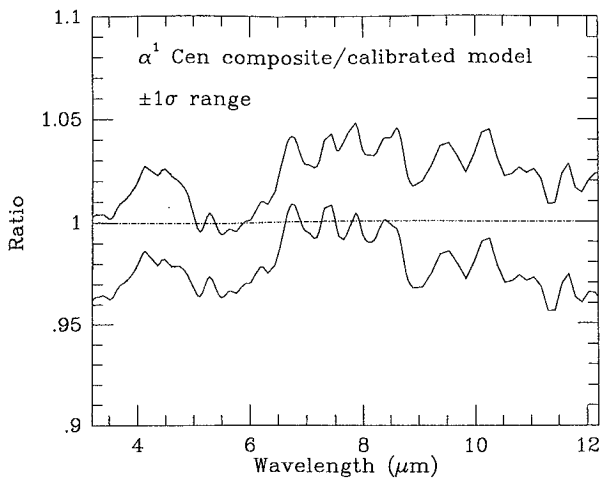

FIG. 4. The ratio of our composite to the calibrated α^1 Cen model in the vicinity of the CO fundamental. The $\pm 1\sigma$ range around the observations is shown and this plot was constructed from the smoothed spectra shown in Fig. 3.

model shape to serve as a smooth interpolator, and plausible extrapolator, of our observations.

To achieve an absolutely calibrated version of the adopted model for α^1 Cen we have directly spliced (by our standard technique: see Papers II and IV) the part of our composite spectrum that is observed (as opposed to that represented by the best-fitting Engelke function) to the model, namely, the 3.0–12.1 μm range. The best-fit scaling factor yields an equivalent angular diameter of 8.58 ± 0.01 mas (the error is determined simply from the χ^2 parabola and represents only the internal precision of this operation). Exactly the same value results from a splice of the model, smoothed by a Gaussian of FWHM 0.2 μm, to an identically smoothed version of the observed spectrum.

To sample a wider spectral range we have also normalized the model to photometry of α^1 Cen in characterized system passbands (see Sec. 3 above). Because we have a continuous model spectrum between 1 and 200 μm and are no longer limited to small fragments within the 3–30 μm region, we have chosen to use all Carter's high-precision measurements for the *JHKL* region, supplemented by the three *ESO* 10 μm narrowbands (*N*1, *N*2, and *N*3: Bouchet *et al.* 1989). After correction for zero points, the actual photometry we used, that does not already appear in Table 2, is: *SAAO-J* -1.138 ± 0.005, *SAAO-H* -1.470 ± 0.005, *SAAO-K* -1.524 ± 0.009, and *ESO-N3* -1.596 ± 0.057. The scaling factor resulting from this normalization is equivalent to an angular diameter of 8.57 ± 0.04 mas (internal precision); an excellent, and somewhat independent accord (because only half the photometry was used to build the composite for α^1 Cen), with that found by comparison of the observed and modeled energy distributions. This compares extremely favorably with the value of 8.62 ± 0.23 mas, derived by Blackwell & Shallis (1977), by application of the IRFM (based on a stellar atmosphere code but not on Kurucz models), but using heterogeneous infrared photometry with diverse absolute calibrations.

It is noteworthy that one can challenge the shape of a model's emergent spectrum solely by use of infrared continuum photometry, provided that one has photometry available over a sufficiently wide range of wavelengths. For example, we experimented with generic Kurucz (1991, 1993a) spectra for F2 V and K2 V stars by testing how well they fitted the actual photometry for α^1 Cen. The relevant parameter is, of course, the bias of the scale factor as one compares the set of in-band fluxes derived from integration over the spectra with those from the independently secured and calibrated ground-based photometric measurements. We found that, while the bias of the best fit of our adopted model for α^1 Cen to this photometry is only about 0.5%, the F and K dwarfs yielded biases of order 3%–4%, substantially poorer. The need for a broad wavelength range arises because of the sensitivity in the computed shapes of stellar infrared energy distributions to effective temperature, which can be measured principally by comparing the *J* band with photometry in the 10 μm window. This sensitivity of real stars and of computed model atmospheres can also be recognized as one of the shortcomings of the Engelke function. In Paper IV one can see how every Engelke approximation predicts far too much flux at wavelengths below about 2 μm because of the analytic oversimplification. While we advocate the selection of relevant theoretical models through use of observed and continuous infrared spectroscopy, it is possible that this rather simplistic approximation could yield adequate results ($\pm10\%$ in irradiance values) for the establishment of rough and ready "standards" in the total absence of any infrared spectroscopy, at least at long infrared continuum wavelengths (cf. Fig. 1).

We conclude that the absolutely calibrated version of our model for α^1 Cen represents the angular diameter of this star as 8.58 ± 0.13 mas, where the uncertainty now includes the external error that arises from the fundamental uncertainty of 1.46% in our Sirius absolute calibration (Paper I). The global bias associated with the calibrated α^1 Cen model is 1.464%. Figure 5 presents the absolutely calibrated model of α^1 Cen in the same format, and on the same wavelength scale, as the models of Vega and Sirius that we showed in Paper I.

There seems to be no direct measurement of α^1 Cen's apparent angular diameter, by an intensity interferometer, presumably because of its binarity and the resulting complex visibility curves. However, there are two recent values for its physical radius determined through atmospheric modeling for an effective temperature of 5770 K. These are 1.21 ± 0.02 $R_\odot$ (Kjellsen & Bedding 1995) and 1.24 ± 0.025 $R_\odot$ (Lydon *et al.* 1990). The most precise parallax is that by Demarque *et al.* (1986: $0.7506\pm0.0046''$). From the implied distance to the star these two radii yield apparent angular diameters of 8.45 ± 0.15 and 8.66 ± 0.19 mas, respectively, where these errors are the root-sum-square combination of the error in the parallax and that in the estimated stellar radius. Combining these results with the diameter of Blackwell & Shallis (1977), using inverse variance weighting, implies that the literature supports a value of 8.55 ± 0.11 mas, vindicating our own estimate.

Therefore, we conclude that both our observed α^1 Cen spectrum, calibrated from our Sirius spectrum, and the shape of our adopted, plausible, independently calculated, α^1 Cen model spectrum are in good agreement (well within 1σ) with

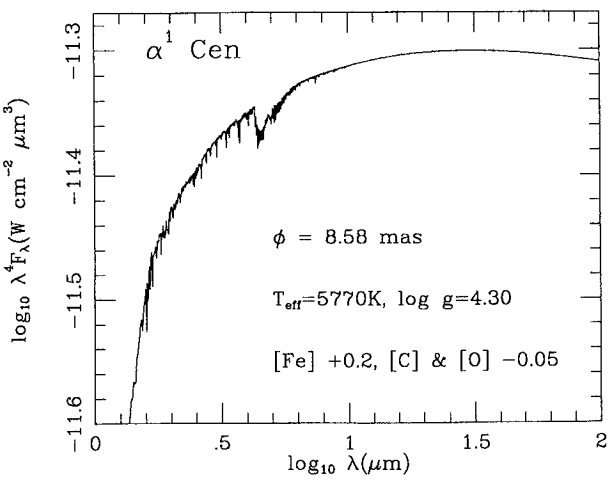

FIG. 5. The adopted, calibrated, theoretical shape for α^1 Cen. Wavelength scale is identical to that used in Paper I to portray our calibrated Vega and Sirius spectra.

infrared photometry and with estimates of the stellar angular diameter. Consequently, this provides an effective closure within our scheme of calibrated infrared spectra, as well as offering a brighter reference star with which to calibrate objects observed in the southern hemisphere.

5. THE LONG-WAVELENGTH SPECTRA

In reality, all our long-wave spectra lacked enough signal-to-noise to use as spectral fragments in their entirety and we resorted instead to combining the data from all the channels on the Si:Bi array and similarly from all the Si:P detectors. To increase signal-to-noise further, we also combined the ratio spectra from all the Si:Bi and Si:P detectors. By this means we were able to derive pseudophotometric points to check our assembled complete spectra because these long-wavelength data were not used in the process of spectral assembly. These photometric points were then converted to flux densities via our calibrated models for Sirius and α^1 Cen. Although the spectra were noisy, we still applied our usual techniques to these spectral fragments, bringing together overlapping ranges by routine splices and augmenting the formal photometric errors by root-sum-squaring with the associated uncertainties (biases) in scale factors for the best overlaps. It is these latter uncertainties that increase the final errors even after combining all the Si:Bi or all the Si:P detectors into a single number, but the methodology is then consistent throughout our work.

We compared α^1 Cen directly to α CMa but were able to use ratios with respect to α^1 Cen and to α CMa for the two K giants, using the absolutely calibrated α^1 Cen spectrum in Fig. 5. The binned long-wave spectral ratios yielded flux densities across the Si:Bi (15.0–18.5 μm) and Si:P (19.5–27.2 μm) ranges. Table 5 summarizes these flux densities for the stars discussed in this paper, indicating which calibrator was used. These flux densities are plotted in Fig. 1 along with the photometry used to assemble the composite spectrum, and the *IRAS* flux densities. Note that although the long-wavelength *KAO* and the *IRAS* data were not used to construct any of these spectral composites they are in good agreement (within 1σ) with our calibrated spectra, as is the *ESO-N3* point for α^1 Cen. To present the *IRAS* flux densities we used the somewhat more precise *IRAS* Faint Source Survey photometry. All the measurements beyond 15 μm are consistent with our extrapolated Engelke functions. The uncertainties in the observed photometry points are rather large but suffice to preclude any radical departures of real stellar spectra from a Rayleigh–Jeans slope within our observed wavelength range.

6. CONCLUSIONS

We have assembled absolutely calibrated, complete, continuous stellar spectra between 3 and 30 μm for three stars: α^1 Cen, α TrA, and ϵ Car. We have created an absolutely calibrated theoretical emergent spectrum derived from Kurucz model atmospheres for α^1 Cen, whose shape is in agreement with our observations of this star. We recommend use of this star when a southern spectral standard brighter than Sirius is needed. The two K giants show deep absorptions of CO and SiO. Our long-wave *KAO* measurements, and those from *IRAS*, are consistent with our extrapolations of observed but noisy stellar spectra by means of the Engelke

TABLE 5. Long-wavelength (>15.00 μm) flux densities derived from the absolutely calibrated α^1 Cen and/or α CMa models.

Star	Data	$\langle\lambda\rangle$ (μm)	$\lambda^4 F_\lambda$ (W cm^{-2} μm^{-1})	$\pm\epsilon(\lambda^4 F_\lambda)$ (W cm^{-2} μm^{-1})	Calibrator
α^1 Cen	Si:Bi	17.30	5.79E-17	0.60E-17	α CMa
α^1 Cen	Si:P	22.50	1.96E-17	0.42E-17	α CMa
α^1 Cen	All	19.90	3.29E-17	0.32E-17	α CMa
α TrA	Si:Bi	16.83	5.79E-17	0.52E-17	α^1 Cen
α TrA	Si:P	24.29	1.40E-17	0.13E-17	α^1 Cen
α TrA	All	20.50	2.69E-17	0.17E-17	α^1 Cen
α TrA	All	20.50	2.17E-17	0.27E-17	α CMa
α TrA	All	20.50	2.54E-17	0.14E-17	α^1 Cen and α CMa
ϵ Car	Si:Bi	17.06	8.41E-17	1.15E-17	α^1 Cen
ϵ Car	Si:P	23.18	2.64E-17	0.28E-17	α^1 Cen
ϵ Car	All	20.12	4.54E-17	0.43E-17	α^1 Cen
ϵ Car	All	19.86	5.75E-17	0.63E-17	α CMa
ϵ Car	All	20.00	4.98E-17	0.36E-17	α^1 Cen and α CMa

approximation; i.e., the energy distributions of cool giants in this mid-infrared region are close to their Rayleigh–Jeans slopes.

We are deeply grateful to Dr. R. Kurucz for generating the mini-grid of model atmospheres that underpin our work on α^1 Cen, for creating the special computations necessary to compare his model with the ATMOS data, and for many valuable discussions concerning our work. It is likewise a pleasure to acknowledge Dr. D. Carbon for a wealth of vital advice, and Dr. B. Carter for obtaining the precision photometry used to construct our composite spectra. M.C. thanks Phillips Laboratory for its support of this effort through Dr. S. D. Price under Contract No. F19628-92-C-0090 with JS&E, Inc. We are grateful to NASA's Airborne Astronomy program and to the entire staff of the *KAO* for their sterling efforts throughout the flights dedicated to this calibration study. M.C. also thanks NASA-Ames Research Center for partial support under Co-Operative Agreement NCC 2-142 with Berkeley. This research has made use of the SIMBAD database, operated at CDS, Strasbourg, France.

REFERENCES

Bell, R. A. 1994, MNRAS, 268, 771
Bell, R. A., & Briley, M. M. 1991, AJ, 102, 763
Bell, R. A., Briley, M. M., & Norris, J. E. 1992, AJ, 104, 1127
Bessell, M. S., & Brett, J. M. 1988, PASP, 100, 1134
Blackwell, D. E., Lynas-Gray, A. E., & Petford, A. D. 1991, A&A, 245, 567
Blackwell, D. E., & Shallis, M. J. 1977, MNRAS, 180, 177
Bouchet, P., Moneti, A., Slezak, E., Le Bertre, T., & Manfroid, J. 1989, A&AS, 80, 379
Carter, B. 1994 (private communication)
Chmielewski, Y., Friel, E., Cayrel de Strobel, G., & Bentolila, C. 1992, A&A, 263, 219
Cohen, M., Walker, R. G., Barlow, M. J., & Deacon, J. R. 1992, AJ, 104, 1650 (Paper I)
Cohen, M., Walker, R. G., & Witteborn, F. C. 1992, AJ, 104, 2030 (Paper II)
Cohen, M., Witteborn, F. C., Walker, R. G., Bregman, J., & Wooden, D. 1995, AJ, 110, 275 (Paper IV)
Demarque, P., Guenther, D. B., & van Altena, W. F. 1986, ApJ, 300, 773
van Dijsseldonk 1994 (private communication)
Engelke, C. W. 1992, AJ, 104, 1248
Engels, D., Sherwood, W. A., Wamsteker, W., & Schultz, G. V. 1981, A&AS, 45, 5
Farmer, C. B., & Norton, R. H. 1989, A High-Resolution Atlas of the Infrared Spectrum of the Sun and Earth Atmosphere from Space, NASA RP-1224
Furenlid, I., & Meylan, T. 1990, ApJ, 350, 827
Goorvitch, D. 1994, ApJS, 95, 535
Harper, G. M. 1992, MNRAS, 256, 37
Hoffleit, D. 1982, Yale Bright Star Catalog, 4th ed. (Yale University Obs., New Haven)
Kirby-Docken, K., & Liu, B. 1978, ApJS, 36, 359
Kjeldsen, H., & Bedding, T. R. 1995, A&A, 293, 87
Kovacs, N. 1983, A&A, 120, 21
Kurucz, R. L. 1991, New lines, new models, new colors, in Precision Photometry: Astrophysics of the Galaxy, edited by A. G. Davis Philip, A. R. Upgren, and K. A. Janes (Davis, Schenectady), p. 27
Kurucz, R. L. 1993a, ATLAS9 Stellar Atmosphere Programs and 2 km/s grid, Kurucz CD-ROM No. 13
Kurucz, R. L. 1993b, SYNTHE Spectrum Synthesis Programs and Line Data, Kurucz CD-ROM No. 18
Kurucz, R. L. 1995 (private communication)
Kurucz, R. L. 1996 (private communication)
Lord, S. D. 1992, A New Software Tool for Computing the Earth's Atmospheric Transmission of Near-Infrared and Far-Infrared Radiation, NASA TM-103957
Lydon, T. S., Fox, P. A., & Sofia, S. 1993, ApJ, 413, 390
Moshir, M., *et al.* 1992, Explanatory Supplement to the *IRAS* Faint Source Survey, Version 2, JPL D-10015 (JPL, Pasadena)
Pasquini, L., & Brocato, E. 1992, A&A, 266, 340
Strecker, D. W., Erickson, E. F., & Witteborn, F. C. 1979, ApJS, 41, 501
Thomas, J. A., Hyland, A. R., & Robinson, G. 1973, MNRAS, 165, 201
Wesselink, A. J., Paranya, K., & DeVorkin, K. 1972, A&AS, 7, 257
Witteborn, F. C., Cohen, M., Bregman, J. D., Heere, K. R., Greene, T. P., & Wooden, D. H. 1995, in Proceedings of the Airborne Astronomy Symposium on the Galactic Ecosystem, ASP Conf. Ser. 73, edited by M. Haas, E. F. Erickson, and J. Davidson (ASP, San Francisco), p. 573